Research Article

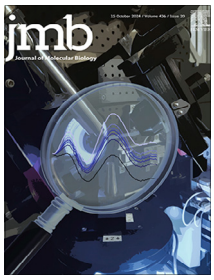

The Phosphatase RosC from *Streptomyces davaonensis* is Used for Roseoflavin Biosynthesis and has Evolved to Largely Prevent Dephosphorylation of the Important Cofactor Riboflavin-5′-phosphate

Tanya Joshi [1], Ulrike Demmer [2], Carmen Schneider [1], Theresa Glaser [1], Eberhard Warkentin [2], Ulrich Ermler [2] and Matthias Mack [1,*]

*1 - **Institute for Technical Microbiology,** Department of Biotechnology, Mannheim University of Applied Sciences, 68163 Mannheim, Germany*

*2 - **Max-Planck-Institute for Biophysics,** Max-von-Laue-Strasse 3, 60438 Frankfurt am Main, Germany*

***Correspondence to Matthias Mack:** m.mack@hs-mannheim.de (M. Mack)*

https://doi.org/10.1016/j.jmb.2024.168734

Edited by Anthony Maxwell

Abstract

The antibiotic roseoflavin is a riboflavin (vitamin B_2) analog. One step of the roseoflavin biosynthetic pathway is catalyzed by the phosphatase RosC, which dephosphorylates 8-demethyl-8-amino-riboflavin-5′-phosphate (AFP) to 8-demethyl-8-amino-riboflavin (AF). RosC also catalyzes the potentially cell-damaging dephosphorylation of the AFP analog riboflavin-5′-phosphate also called “flavin mononucleotide” (FMN), however, with a lower efficiency. We performed X-ray structural analyses and mutagenesis studies on RosC from *Streptomyces davaonensis* to understand binding of the flavin substrates, the distinction between AFP and FMN and the catalytic mechanism of this enzyme. This work is the first structural analysis of an AFP phosphatase. Each monomer of the RosC dimer consists of an α/β-fold core, which is extended by three specific elongated strand-to-helix sections and a specific N-terminal helix. Altogether these segments envelope the flavin thereby forming a novel flavin-binding site. We propose that distinction between AFP and FMN is provided by substrate-induced rigidification of the four RosC specific supplementary segments mentioned above and by an interaction between the amino group at C8 of AFP and the β-carboxylate of D166. This key amino acid is involved in binding the ring system of AFP and positioning its ribitol phosphate part. Accordingly, site-specific exchanges at D166 disturbed the active site geometry of the enzyme and drastically reduced the catalytic activity. Based on the structure of the catalytic core we constructed a whole series of RosC variants but a disturbing, FMN dephosphorylating “killer enzyme”, was not generated.

Introduction

Roseoflavin (8-demethyl-8-dimethylamino-riboflavin) is the only known natural riboflavin (vitamin B_2) analog with antibiotic function.[1,2] Roseoflavin is produced by the bacteria *S. davaonensis*, *Streptomyces cinnabarinus* and *Streptomyces berlinensis*, the latter just recently being described as a novel roseoflavin producing species.[3] The biosynthetic pathway of roseoflavin (Figure 1) starts with FMN which in turn is generated by the flavokinase function of the bifunctional flavokinase (EC 2.7.1.26)/flavin adenine dinucleotide (FAD) synthetase (EC 2.7.7.2) RibCF from riboflavin and

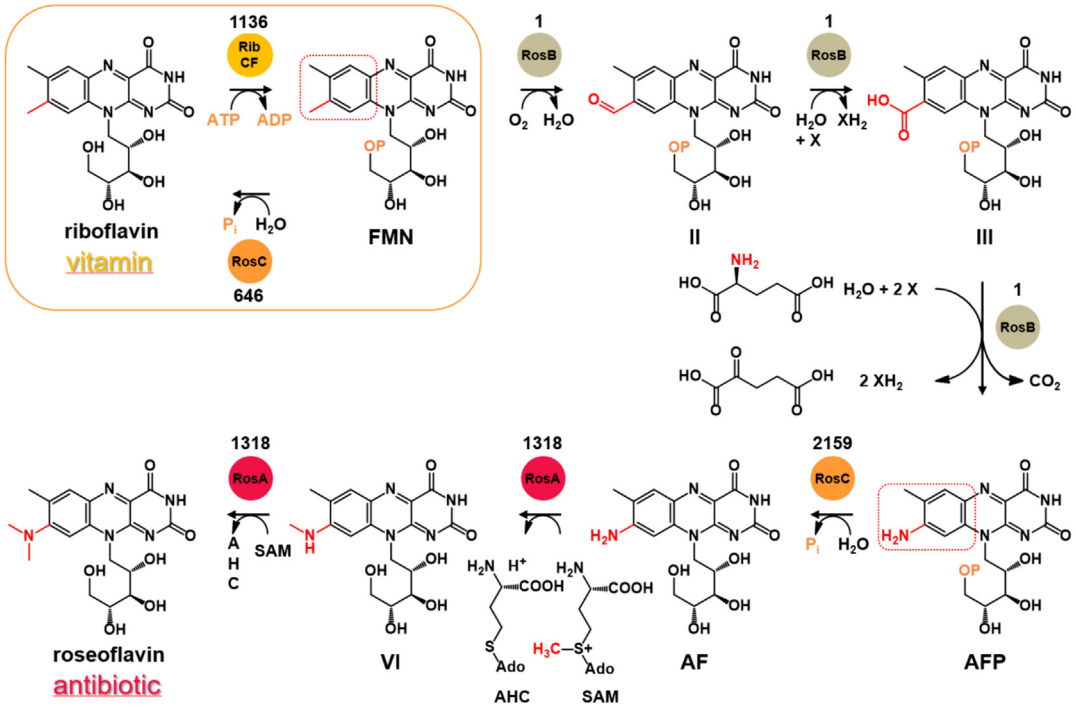

Figure 1. Biosynthesis of the antibiotic roseoflavin in the bacteria *Streptomyces davaonensis*, Streptomyces cinnabarinus and Streptomyces berlinensis. Enzymes (circles) and their relative rates (normalized to the slowest enzyme of the pathway, RosB) are shown.[5,8] Phosphates are shown in orange. RosC (orange circle) dephosphorylates 8-demethyl-8-amino-riboflavin-5′-phosphate (AFP) as AFP is not a substrate for RosA. A possible "futile cycle" is indicated by a dotted orange box as RosC also dephosphorylates FMN (albeit at a lower rate). FMN, riboflavin-5′-phosphate or flavin mononucleotide. II, 8-demethyl-8-formyl-riboflavin-5′-phosphate. III, 8-demethyl-8-carboxyl-riboflavin-5′-phosphate. AF, 8-demethyl-8-amino-riboflavin. VI, 8-demethyl-8-methylamino-riboflavin. The methyl group donor is S-adenosyl methionine (SAM) and as a side-product S-adenosylhomocysteine (AHC) is formed. The structural similarity of FMN and AFP is high-lighted by a red box (dotted line). RosC activity was determined in this work by monitoring formation of AF from AFP by HPLC-DAD.

ATP.[4] In three steps FMN is converted to AFP by the complex synthase RosB (EC 2.6.1.114).[5,6] We showed in a previous structural work that RosB has evolved from a hydride-transferring flavodoxin to a sophisticated multi-step enzyme.[7] The phosphatase RosC (EC 3.1.3.-) dephosphorylates AFP to AF[8] which in two steps finally is converted to roseoflavin by the *N*,*N*-dimethyltransferase RosA (EC 2.1.1.343).[9] In roseoflavin biosynthesis riboflavin is first phosphorylated by RibCF to FMN, and, further down the pathway, the phosphate group of the intermediate AFP is again removed by RosC (Figure 1). When compared to RosB (0.44 nmol min^{-1} mg^{-1}), RosC has a 2159× higher specific activity (0.95 μmol min^{-1} mg^{-1}).[8] It is reasonable to assume that RosC-mediated dephosphorylation of AFP drives the roseoflavin pathway explaining why FMN (and not riboflavin) is used as the starting point of roseoflavin biosynthesis.[8] AFP and the important cellular cofactor FMN are highly similar and differ only with regard to the substituents at C8 of the benzene ring (Figure 1). Phosphorylation of riboflavin by RibCF in combination with dephosphorylation of FMN by RosC would generate a "futile cycle" (Figure 1) and indeed AFP (V_{max} = 0.95 μmol min^{-1} mg $protein^{-1}$, K_M = 34.5 μM) is a better substrate for RosC than FMN (V_{max} = 0.21 μmol min^{-1} mg $protein^{-1}$, K_M = 309 μM).[8] We report here on the three-dimensional structure of the AFP phosphatase RosC focusing on the architecture of a novel flavin binding site, the catalytic mechanism of AFP dephosphorylation and the important physiological discrimination between AFP and FMN.

Results

AFP phosphatases are only present in roseoflavin producing microorganisms

RosC (222 amino acids; 25.58 kDa) belongs to the superfamily of histidine phosphatases and amino acids 28–210 of *S. davaonensis* RosC share up to 50% identity with other family members.[8] In contrast, the N-terminus of RosC (amino acids 1–22) was found in the roseoflavin producing bacteria *S. davaonensis*, *S. cinnabarinus*

and *S. berlinensis* only and we hypothesized that these amino acids (in addition to other parts of the enzyme) would represent a specific adaptation to roseoflavin biosynthesis. The finding that in the genomes of *Streptomyces* sp. NBRC 14336 and *Streptomyces* sp. HUAS putative *rosC* genes were present strongly suggested that these isolates were producers of roseoflavin as well.[3] These strains are not available through public strain collections and thus could not be studied with regard to roseoflavin biosynthesis. In *Streptomyces* sp. HUAS an enzyme similar to RosB was found. RosA, however, was not found suggesting that *Streptomyces* sp. HUAS is a producer of AF and does not carry out the final, RosA-catalyzed dimethylation reaction to generate roseoflavin. Primary structure alignments now show that AFP phosphatases (including those of *Streptomyces* sp. NBRC 14336 and *Streptomyces* sp. HUAS) all contain a highly conserved N-terminal extension comprising 22 amino acids (Figure S1) and three pronounced sections I, II and III, which are unique to AFP phosphatases and are not present in other histidine phosphatases (Figure S2).

Overproduction, purification and X-ray structure analysis of recombinant S. davaonensis RosC and variants thereof

The previously reported overproduction/purification procedure for *S. davaonensis* RosC based on the expression plasmid pPSG-IBA3 and the host *E. coli*[8] yielded protein in quantities insufficient to sample a wide range of crystallization spaces for structural analysis and kinetic studies. The amount of recombinant protein obtained was very small and purification was laborious. A novel procedure based on a newly constructed *E. coli* strain employing the expression plasmid pET28a (instead of pPSG-IBA3) was developed in this work and yielded sufficient amounts of pure RosC. Based on this procedure RosC wild-type (Figure S3) and 26 RosC variants were purified to apparent homogeneity and kinetically characterized (Table 1) by an *in vitro* AFP phosphatase assay. X-ray structures were determined of (1) flavin-free RosC, (2) RosC in complex with the reaction product AF ("RosC-AF"), (3) RosC in complex with AF and inorganic phosphate (mimicking RosC in complex with the substrate AFP) and (4) the RosC variant $RosC^{R33A}$ (in which arginine 33 was replaced by alanine) in complex with riboflavin ("$RosC^{R33A}$-riboflavin") (Table S1). We were not successful in crystallizing RosC in complex with the substrate AFP, most likely due to dephosphorylation of AFP by the enzyme during crystallization.

The X-ray structure of flavin-free wild-type RosC determined at 1.7 Å resolution revealed a compact homodimeric enzyme (Figure 2A) which is in line with gel filtration data (Figure S4). Each monomer is built of a mixed six-stranded β-sheet sandwiched between two α-helices which is characteristic for the histidine phosphatase family.[10] In RosC, this core fold is supplemented by the expanded strand-helix sections I (32–54), II (101–132) and III (178–192) and by a 22 amino acid N-terminal helical extension (Figure 2A). Interestingly, the latter is separated from the residual subunit and associates with the partner subunit (Figure 2C; Figure S5). In the flavin-free RosC structure the four supplementary segments and especially the N-terminal helical extension are rather flexible and even partly disordered, which is expressed in a high B-factor (Figure 2B).

Binding of the reaction product AF to the active site of RosC

The structure of RosC-AF at 1.25 Å resolution revealed the product of the dephosphorylation reaction, AF, in a fully occupied state (Figure 2C). AF is arranged in a manner that the tip of the ribityl sits next to the central strand ends of the protein core, from which the remaining flavin extends towards the protein periphery thereby fixed by sections I, II and III and the N-terminal helical extension (Figure 2C). The ring system of AF is enveloped by the N-terminal helical extension of the partner subunit and the extended insertion II, which is kept in its conformation by sections I and III. AF binding changes the positions and conformations of the RosC specific supplementary segments in the range of 2–3 Å to promote interactions with the flavin and with each other, respectively. This substrate-induced rigidification is expressed in strongly reduced B-factors (compare Figure 2B and D). The planar heterocyclic ring system of AF is held in place by P127, F128 and W181 at its *si*-face and V11′, V15′, Y16′ and Y19′ of the N-terminal partner helix at its *re*-face (Figure 3A) (partner subunit residues are labelled with an apostrophe). Interactions between the polypeptide and the polar groups of AF are shown in Figure 3B, whereby those to the C8 amino group of AF and the enzyme are treated in the next section. Site-directed mutagenesis experiments revealed that the RosC variants $RosC^{P127A}$, $RosC^{F128A}$, $RosC^{W181A}$, $RosC^{V11A}$, $RosC^{V15A}$, $RosC^{Y16A}$ and $RosC^{Y19A}$ were either inactive or showed reduced AFP/FMN phosphatase activity validating the importance of these amino acids with regard to flavin binding (Table 1). Some of these variants ($RosC^{F128A}$, $RosC^{Y16A}$ and $RosC^{P127A}$) were analyzed in more detail (Table 2) and the different K_M values for both AFP and FMN indicated a change of binding affinity with regard to the wild-type enzyme. Deletion of the N-terminal helical extension ($RosC^{\Delta 22}$) (see Figure 2C and Figure S5) led to an insoluble RosC variant, which could not be

Table 1 **A series of RosC variants was constructed, purified to apparent homogeneity and tested with the flavin substrates 8-demethyl-8-amino-riboflavin-5′-phosphate (AFP) and riboflavin-5′-phosphate (flavin mononucleotide or FMN).** The specific activity was measured in an assay containing 200 μM flavin substrate and 0.1–1 μM enzyme (depending on the RosC variant).

RosC variant	Specific activity (AFP) μmol min-1 mg^{-1}	Specific activity (FMN) μmol min-1 mg^{-1}	Relative activity with regard to $RosC^{WT}$ for AFP (%)	Relative activity with regard to $RosC^{WT}$ for FMN (%)
Wild-type	0.95 ± 0.06	0.21 ± 0.02	100	100
P127A	0.051 ± 0.00245	[a]–	5.3	–
F128A	0.024 ± 0.002	0.0032 ± 0.004	2.5	1.5
W181A	0.029 ± 0.0024	–	3	–
V11A	0.55 ± 0.021	0.021 ± 0.02	57.8	10
V15A	1.01 ± 0.010	0.0142 ± 0.005	106.3	6.7
Y16A	0.46 ± 0.005	0.044 ± 0.022	48.4	20.9
Y19A	0.69 ± 0.03	0.026 ± 0.014	7.2	12.3
$RosC^{\Delta 22}$-MBP	–	–	–	–
RosC-MBP	0.38 ± 0.009	0.0976 ± 0.007	40	46.4
G22P	–	–	–	–
G25P	–	–	–	–
D166L	0.006 ± 0.0004	0.0073 ± 0.0004	0.6	3.5
D166I	–	–	–	–
D166V	–	–	–	–
D166A	0.12 ± 0.014	–	12.6	–
D166T	–	–	–	–
D166N	0.0318 ± 0.003	0.0291 ± 0.0037	3.3	13.8
M186A	0.0016 ± 0.0001	–	0.17	–
D166G	0.427 ± 0.057	0.088 ± 0.029	45	42
D166E	1.5 ± 0.045	0.567 ± 0.026	157.8	283.5
H34A	0.02	n.d.	[b]2.2	n.d.
R33A	0.007	n.d.	[b]0.7	n.d.
R83A	0.008	n.d.	[b]0.8	n.d.
E107A	–	–	–	–
E107Q	0.0016 ± 0.0002	0.0016 ± 0.0002	0.1	0.1
Y38A	0.167 ± 0.009	0.0046 ± 0.0014	17.4	2.2
H82A	1.06	n.d.	[b]111.6	n.d.
V170I	0.793 ± 0.095	0.1956 ± 0.008	83.4	92.8
E119A	0.58 ± 0.016	0.0515 ± 0.005	61	24.5
K121A	0.55 ± 0.06	0.091 ± 0.006	57.8	43.3
H165A	0.0019	n.d.	[b]0.2	n.d.
H34A + H165A	–	–	–	–
F8A	0.67 ± 0.049	0.016 ± 0.0002	70.5	7.6

[a] "–" means "no activity".
[b] Data taken from an earlier publication.[34]

purified using the standard procedure. However, a soluble protein was obtained by generating an N-terminal fusion of $RosC^{\Delta 22}$ to the maltose binding protein (MBP) of *E. coli* (Figure S6). The fusion protein $RosC^{\Delta 22}$-MBP still formed a dimer (Figure S4) showing that the N-terminal helix is not crucial for oligomerization. $RosC^{\Delta 22}$-MBP neither catalyzed dephosphorylation of AFP nor of FMN (Table 1) validating the importance of the N-terminal extension with regard to substrate binding. The amino acids G22 and G25 localized at the hinge between the protein core and the N-terminal helix (Figure S7) were replaced by proline, which resulted in the completely inactive RosC variants $RosC^{G25P}$ and $RosC^{G22P}$ (Table 1). These data suggest that the flexible glycine residues at this position are crucial for the mobility of the N-terminal helix and its positioning relative to the partner subunit.

The amino acid residue D166 within RosC confers AFP specificity

Analysis of the RosC-AF structure revealed that the environment of the amino group at C8 of AF plays an outstanding role with regard to the specificity of RosC towards AFP. The amine at C8 of AF interacts with the carbonyl oxygen of M186 and with a β-carboxylate oxygen of D166 (Figure 3A). The oxygen atoms OD1 and OD2 of the β-carboxylate of D166 in turn are firmly held in their positions by interactions with L188-NH and

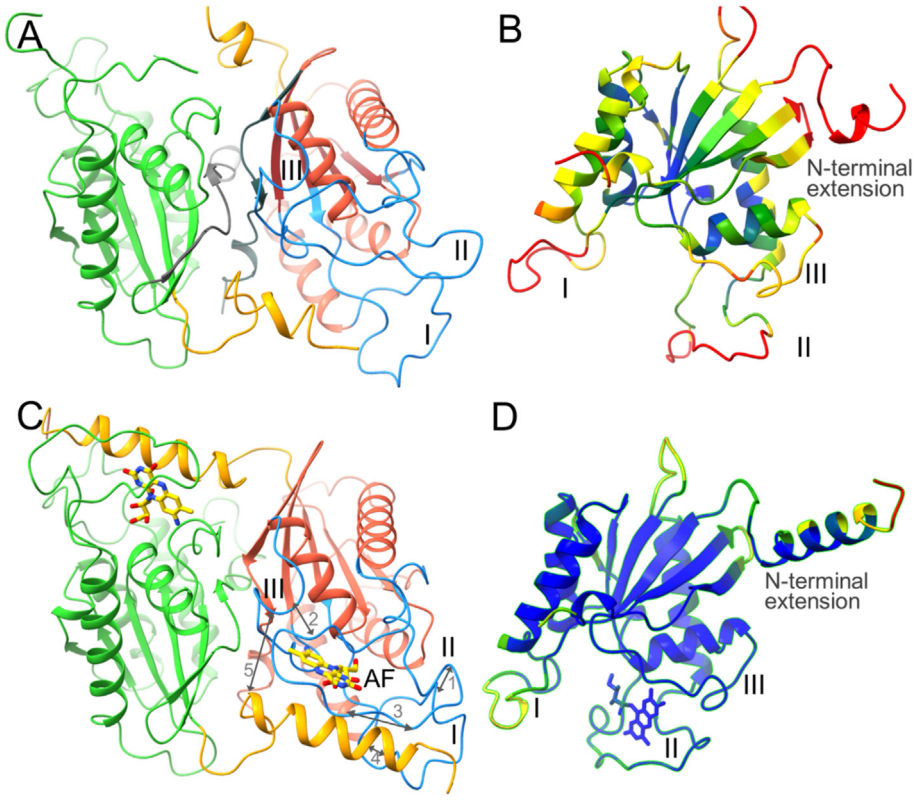

Figure 2. Crystal structures of the 8-demethyl-8-amino-riboflavin-5′-phosphate (AFP) phosphatase RosC from *Streptomyces davaonensis*. A. The wild-type RosC dimer in the absence of flavins. Each subunit (green and red) is primarily built up of an α/β-fold. The extended homodimer interface is mainly constructed by the N (gold)- and C (dark gray)-terminal segments of the enzyme. Interestingly, the C-terminal β-strands of both subunits (dark gray) connect the two six-stranded β-sheets of the two subunits. Sections I (32–54), II (101–132) and III (178–192) are highlighted in blue. Notably, in the absence of flavins the N-terminal α-helix is largely disordered and is better visible in C. B. B-factor colored RosC monomer (B = 0–25 (blue), 25–50 (green), 50–75 (yellow), >75 (red) Å^2). Sections I-III and the N-terminal α-helix of the flavin-free RosC structure are highly flexible reflected in a high B-factor that describes the attenuation of X-ray scattering caused by thermal motion. C. The RosC-8-demethyl-8-amino-riboflavin (AF) complex. AF is flanked by the three RosC-specific sections I, II and III and the N-terminal helix (gold) of the partner subunit (green). These segments mutually stabilize each other or themselves (marked by gray arrows 1–5). Section II packs against sections I and III by a salt bridge (1) (OD1 of D113 and NH1 of R49) and a hydrophobic patch (Y126, P127, F128 and W181) (2), respectively and multiply against the N-terminal partner helix (segment 7′-18′; partner subunit residues are labelled with an apostrophe) (3). The latter is also linked with sections I and III by a hydrophobic patch (F8′, L9′, M12′, Y38 and L41) (4) and by a hydrogen-bond (OH of Y19′ and OD1 of D185) (5), respectively. D. B-factor colored monomer of the RosC-AF complex (B = 0–25 (blue), 25–50 (green), 50–75 (yellow), >75 (red) Å^2). When compared to the flavin-free structure (B) the B-factors of sections I, II and III and the N-terminal helix of the RosC-AF complex are strongly decreased indicating rigorous rigidification of the four supplementary segments.

the 4′-OH group of the AF ribitol (Figure 3A and B). Using an UV-metric approach the pK_a-value of the C8 amine of free AF was determined to be 1.41 (Figure S8), which suggests a deprotonated and uncharged state at cellular pH. In the protein-bound state the C8 amine might be nevertheless protonated enabled by the presumably deprotonated D166 and delocalization of free electron pairs of the flavin over the macrocyclic ring (Figure S9). Accordingly, a resonance structure of AF with a negative charge at O4A and a positive charge at the iminium ion at C8 (quinonoid form of AF)[11] can be proposed. A negative charge at O4A may be stabilized by the K121 main chain amine and the positively charged side chains of R18 and K121 (Figure 3B and Figure S9). Notably, an under all conditions uncharged C8 methyl of FMN interacts less favorably with D166 which is reflected in the about 9 times higher K_M for FMN (K_M = 309 μM) when compared to AFP (K_M = 34.5 μM).

The importance of D166 (and of M186) with regard to AFP binding was substantiated by characterizing a variety of RosC^{D166} variants,

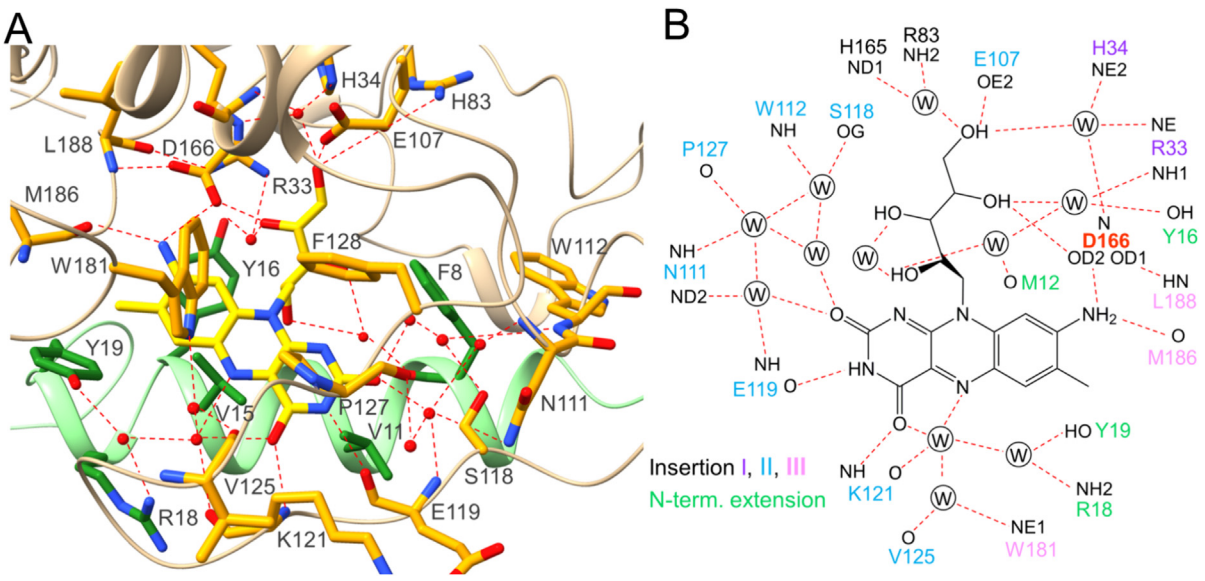

Figure 3. Interactions between RosC and the reaction product 8-demethyl-8-amino-riboflavin (AF). A. Detailed RosC-AF interactions shown in a 3D cartoon representation. Amino acid residues of the two RosC monomers (tan and light green) contacting AF (yellow carbons) are drawn as sticks (carbons in orange or green depending on the subunit origin) and water molecules as red balls. The key amino acid D166 and its contacts to the C8 amine of AF and the hydroxyl of its ribityl are shown in the upper part. B. Schematic representation of the hydrogen-bond network between selected amino acids of RosC and AF. The ribityl and isoalloxazine of AF are characteristically surrounded by the four specific supplementary segments (sections I–III and an N-terminal extension; color coded as shown) thereby constituting a novel flavin binding pocket. Amino acids of linker II (blue) directly or indirectly (*via* water molecules, "circled W") interact with heteroatoms of the polar pyrimidine part of AF.

Table 2 **Determination of steady-state kinetic parameters of RosC and variants thereof for the substrates 8-demethyl-8-amino-riboflavin-5′-phosphate (AFP) and riboflavin-5′-phosphate (flavin mononucleotide or FMN).** Varying amounts of AFP (5–400 μM) and FMN (0–1.000 μM) were incubated in the presence of 0.05–1 μM of the RosC variants. Apparent initial rates were calculated in the linear range of 8-demethyl-8-amino-riboflavin and riboflavin formation and plotted against the substrate concentrations. Kinetic constants K_M and V_{max} were determined by fitting the data to the Michaelis-Menten equation using non-linear regression.

RosC variant	Substrate	V_{max} μmol $min^{-1}mg^{-1}$	K_M μM	k_{cat} min^{-1}
Wild-type	AFP	0.95 ± 0.06	34.5 ± 5.6	31.3
Wild-type	FMN	0.21 ± 0.02	309 ± 61	7.1
F128A	AFP	0.0249 ± 0.001	22.9 ± 8.79	0.7
Y16A	AFP	0.403 ± 0.016	1.8 ± 0.356	10.4
P127A	AFP	0.054 ± 0.001	12.9 ± 1.95	1.4
D166E	AFP	1.57 ± 0.063	11.1 ± 1.96	40.2
D166E	FMN	0.594 ± 0.045	24.5 ± 3.48	15.1
W181A	AFP	0.0379 ± 0.005	69.2 ± 27.6	0.9
Y38A	AFP	0.163 ± 0.059	5.7 ± 0.98	4.2
D166A	AFP	0.11 ± 0.014	39.9 ± 15.26	2.8
V170L	AFP	1.03 ± 0.80	1.3 ± 0.13	26.4
V170L	FMN	0.356 ± 0.028	109.6 ± 17.55	9.1

which (with one exception) exhibited drastically reduced enzyme activities (Tables 1 and 2). Our structural analysis showed that an amino acid exchange at position 166 would not only influence interaction with the amino group of the substrate AFP but also with the ribityl 4′OH of AFP, which is next to the phosphate group to be removed (Figure 3). This dual function explains that variants $RosC^{D166L}$, $RosC^{D166I}$, $RosC^{D166V}$, $RosC^{D166A}$ and also $RosC^{D166T}$ exhibited very low or no dephosphorylation activity when using AFP and also FMN as substrates. Interestingly, in $RosC^{D166L}$ the relative activity for FMN (3.5% of wild-type RosC activity) was higher than that for AFP (0.6% of wild-type RosC activity). This finding can be explained by a more favorable

hydrophobic interaction between the C8 methyl of FMN and the L166 side chain of the variant RosC^{D166L}. The low activity of the RosC^{D166N} variant is surprising as N166 should still be able to interact with the C8 amine and 4′-OH of AF (see Figure 3). RosC^{D166N} lacks the contact to L188 and also the predicted salt bridge between the D166 carboxylate and C8 imine of AF (see above) and, indirectly, the low activity of RosC^{D166N} supports the presence and importance of this salt bridge in the wild-type enzyme. The presence of the D166 carboxylate and C8 imine salt bridge is further substantiated by analysis of the variant RosC^{D166E}, which has an even higher AFP and FMN dephosphorylation activity when compared to the wild-type (158% activity on AFP and 284% on FMN) (Table 1). Apparently, the plasticity of this region is sufficiently high to accommodate one additional methylene group (which is reflected by even lower K_M values for both substrates when compared to the wild-type enzyme; Table 2). This finding is consistent with the earlier finding that roseoflavin-5′-phosphate (RoFMN), which has a bulky dimethylamino group at C8, is also a good substrate for RosC.[8] This activity of RosC in turn may contribute to roseoflavin resistance of the producer *S. davaonensis* as RoFMN negatively affects flavoproteins and thus is toxic.[12,13]

Binding and dephosphorylation of AFP by RosC

The active site of RosC was analyzed on the basis of the structure of the RosC-AF-phosphate complex (Figure 4A). Due to the high resolution (1.55 Å) the positions of the phosphate oxygens

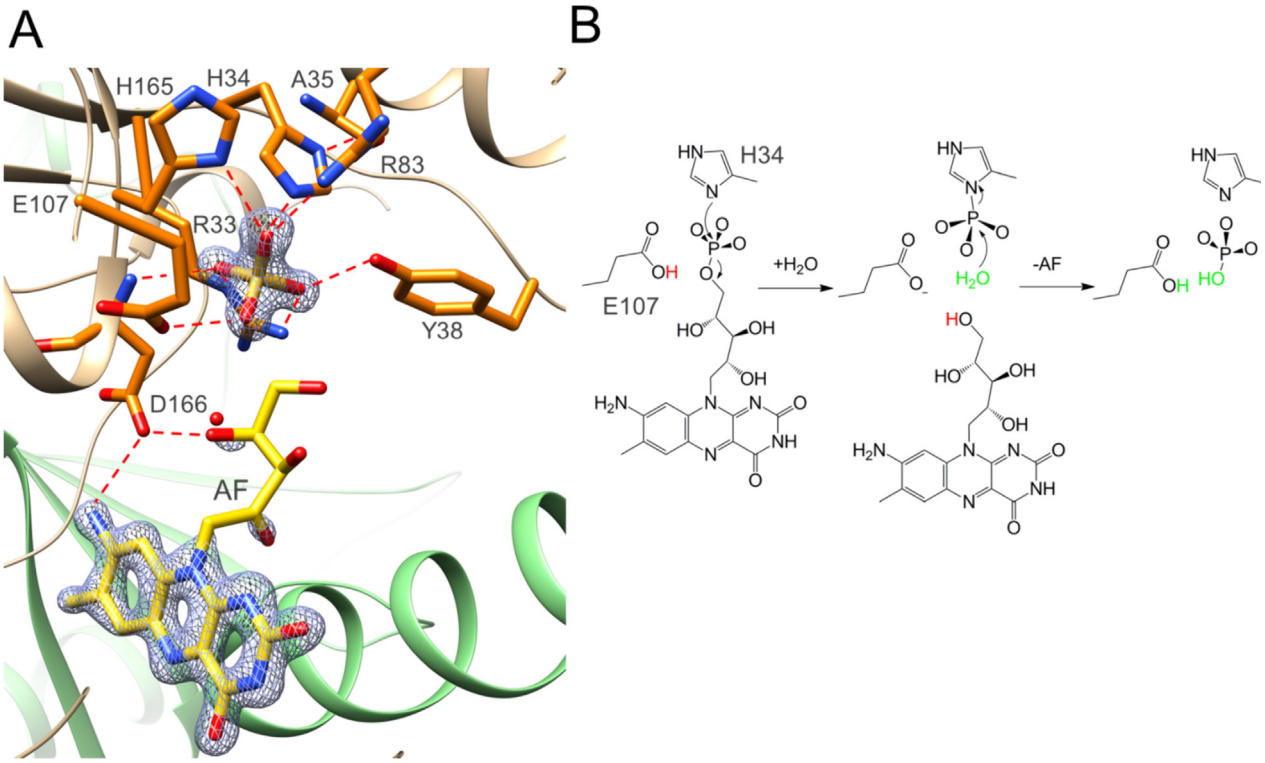

Figure 4. The phosphate binding pocket of the active site of RosC and the catalytic mechanism. A. The RosC-AF-phosphate structure resembles the RosC-AFP and the RosC-AF-phosphate histidine intermediate structures shown in B (middle). The catalytic apparatus of RosC is primarily built of segments which follow the two β-strands 28:32 and 158:163 hosting the phosphate-contacting residues R33, H34, A35, Y38, H165, D166 and R183. B. Catalytic mechanism of the RosC reaction. AFP binds to the softened state of the supplementary segments (see Figure 2B) that allows the bulky substrate to reach its binding site. After a pronounced induced-fit process AFP is almost completely enveloped by the rigidified protein matrix. The imidazole of H34, ideally positioned between the three free oxygens of the AFP phosphate, attacks the phosphorous by an in-line nucleophilic reaction. R33, R83 and H165 fix the phosphate oxygens and stabilize the transition state towards the histidine phosphate intermediate. E107-OD2 with a distance of 2.6 Å to the oxygen bridging the phosphate phosphorous and the ribityl 5′-OH in the substrate is properly placed to serve as proton donor for the released product AF. Most likely a water molecule will occupy the former position of the AF-C5′ hydroxyl group. In the RosC-AF-phosphate structure the most attractive water is about 4.5 Å apart from the phosphate of the H34-phosphate intermediate and might migrate about 1.5 Å in continuous contact with E107 after AF release. The nucleophilic attack of OH^- (E107 accepts a proton from the water molecule) onto the H34-phosphate and the subsequent cleavage of the phosphate histidine bond complete the reaction.

and their hydrogen bonds with H34, H165, R33, R83, E107, Y38, the peptide bond nitrogen of the key amino acid D166 and the 4′ OH of AF could accurately be determined. Following the mechanism postulated for other histidine phosphatases,[10] we propose the following reaction mechanism for the dephosphorylation of AFP by RosC (Figure 4B). The imidazole of RosC H34, pointing towards the phosphorous atom of the phosphate, forms an invariant hydrogen-bond with the carbonyl oxygen of A35 (Figure 4A). In most other histidine phosphatases (Figure S2) this position is occupied by a glycine being part of the strongly conserved signature motif arginine-histidine-glycine (RHG) (Figure S2). The proton donor of the dephosphorylation reaction varies among members of the different histidine phosphatases and is not conserved.[10] In case of RosC, E107 is in an ideal position to serve as proton donor to allow the release of the reaction product AF. The variants $RosC^{H34A}$, $RosC^{H165A}$, $RosC^{R33A}$, $RosC^{R83A}$, $RosC^{E107A}$, $RosC^{E107Q}$, $RosC^{Y38A}$ and $RosC^{D166A}$ showed drastically reduced activities confirming the vital role of each of these residues for catalysis (Table 1). The double mutant $RosC^{H34A/H165A}$ was completely inactive. $RosC^{H82A}$ was used as a "control" as the side chain of H82 is directed away from the active site and was predicted by the InterPro tool to not play a role in catalysis (Figure S10). Indeed, replacement of this amino acid by alanine did not change the activity of RosC (Table 1).

Structural analysis of the $RosC^{R33A}$ variant explains its riboflavin binding capacity

In contrast to wild-type RosC, $RosC^{R33A}$ preparations were yellow when purified from the corresponding recombinant *E. coli* strain. The yellow color was due to riboflavin as shown by HPLC-DAD analysis of the supernatant of denatured $RosC^{R33A}$ preparations (Figure S11). This finding was puzzling as our data described in the preceding section showed that R33 was not involved in binding of the flavin (see Figure 4). For clarification, we solved the X-ray structure of the $RosC^{R33A}$-riboflavin complex (Figure 5A). This structure (1.5 Å resolution) revealed a highly similar flavin binding mode as described for AF in the RosC-AF complex (see Figure 2C) including the extraordinary polypeptide rigidification event upon flavin binding. In the wild-type enzyme R33 is deeply buried, directly involved in phosphate binding and fixed by hydrogen-bonding to a variety of amino acids (see Figure 4). A replacement of the bulky side chain R33 in $RosC^{R33A}$ resulted in a shift of L190 and D166 towards the vacant space which became further occupied by a firmly bound water molecule between D166 and H34 (Figure 5A). When compared to the RosC-wild-type-AF complex (Figure 5B), D166 in the $RosC^{R33A}$-riboflavin complex reorients to the 4′-OH and 5′-OH groups of the flavin ribityl forming two hydrogen-bonds instead of one (Figure 5A). In this conformation the distance between D166-OD2 and the C8-methyl of riboflavin increases from 3.0 Å to 4.2 Å (when compared to D166-OD2 and the C8-amino group of AF in RosC wild-type-AF) and weakens an otherwise unfavorable interaction. The different position of the ribityl phosphate in $RosC^{R33A}$ of course also affects dephosphorylation and explains the reduced activity of this variant. Riboflavin binding to $RosC^{R33A}$ is further supported by side chain rearrangements of I187 and V170 towards the non-polar C8-methyl of the flavin and by a concomitant displacement of its heterocyclic part by 0.5 Å. Due to this shift, the distance between the M186 carbonyl oxygen and the C8-methyl of riboflavin increases from 3.0 Å (RosC-AF complex) to 3.8 Å ($RosC^{R33A}$-riboflavin complex) again weakening an unfavorable interaction. Without major structural arrangements a flavin with a methyl group at C8, such as riboflavin or the cofactor flavin mononucleotide (FMN), would not bind to the active site of RosC.

The RosC variants $RosC^{D166L}$, $RosC^{D166I}$ and $RosC^{D166V}$ are toxic to E. coli and C. glutamicum

Although the RosC wild-type enzyme and the RosC variant $RosC^{D166E}$ (and $RosC^{D166N}$) dephosphorylate FMN, growth reduction of recombinant *E. coli* strains upon induction of these proteins was not observed. However, growth was greatly reduced in recombinant *E. coli* strains upon induction of $RosC^{D166L}$, $RosC^{D166I}$ and $RosC^{D166V}$ (Figure 6). The cells overproducing $RosC^{D166L}$ could not be rescued by adding a vitamin mixture (also containing riboflavin and FMN), a trace element solution or casamino acids. $RosC^{D166L}$ was also induced in the bacteria *Bacillus subtilis* and *C. glutamicum*. The growth reducing effect of $RosC^{D166L}$ was observed in *C. glutamicum* but not in *B. subtilis* (Figure 7). In cell-free extracts of *E. coli* and *C. glutamicum* $RosC^{D166L}$ could not be detected by SDS-PAGE upon induction (Coomassie blue staining) which gives support to the finding that this RosC variant is toxic (Figure S12). In case of *E. coli* induction of $RosC^{D166L}$ was verified by Western-blot analysis (Figure S13) whereby the very low levels of $RosC^{D166L}$ in the host cell were in line with the high toxicity of this protein. In *B. subtilis* $RosC^{D166L}$ could be detected by SDS-PAGE upon induction. However, when compared to wild-type RosC, less $RosC^{D166L}$ was produced suggesting a minor toxic effect of this protein also in *B. subtilis*. The strongly reduced phosphatase activity of $RosC^{D166L}$, $RosC^{D166I}$ and $RosC^{D166V}$ when compared with the wild-type enzyme (Table 1) excludes a drastic reduction of the FMN/FAD

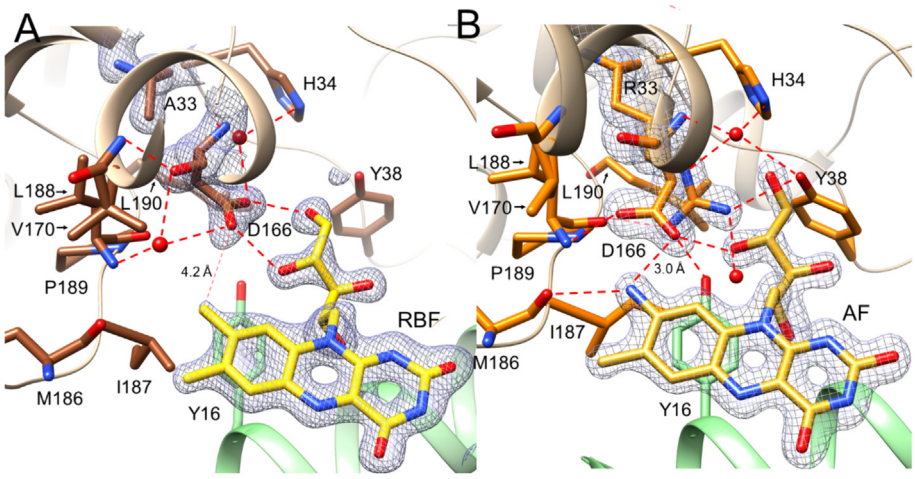

Figure 5. Binding of riboflavin to the variant RosC^{R33A}. A. Structure of the RosC^{R33A}- riboflavin complex at 1.5 Å resolution. D166 evades the C8 methyl of riboflavin and, in contrast to the wild-type enzyme, interacts with two hydroxyl groups at C4′ and C5′ of the ribityl part (red dashed line). This conformational change is enabled by the space created by replacing the bulky arginine at position 33 by alanine (A33). B. The RosC-8-demethyl-8-amino-riboflavin (AF) structure for comparison. D166 interacts with the amino group at C8 of the AF isoalloxazine.

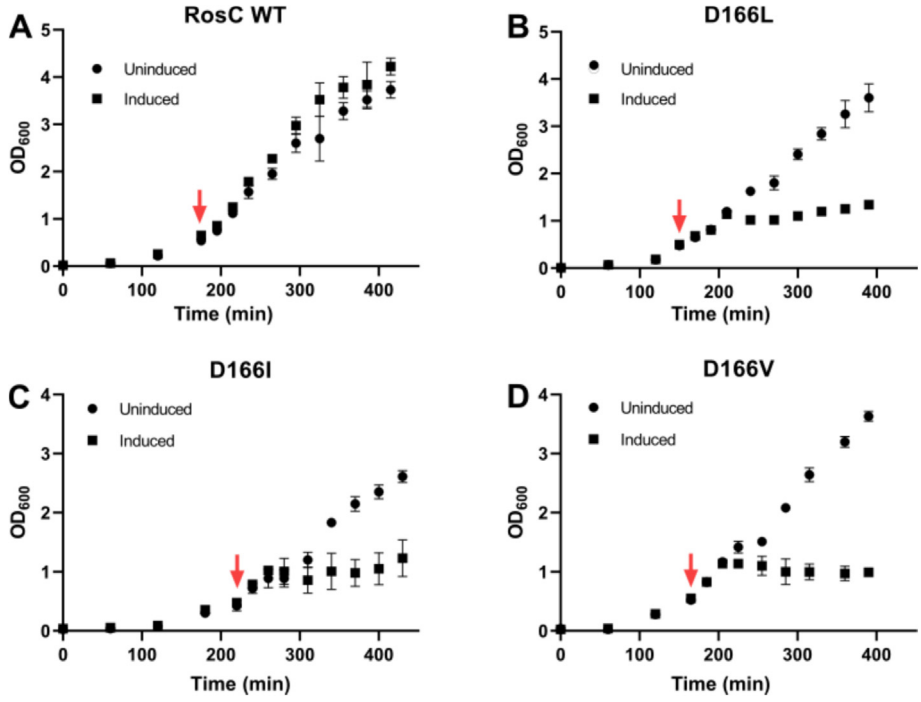

Figure 6. Growth was greatly reduced in recombinant *Escherichia coli* strains that overproduced RosC^{D166L}, RosC^{D166I} and RosC^{D166V}. Growth of *E. coli* strains containing plasmids that enable overexpression of the *rosC* wild-type gene and variants was monitored. The red arrow shows the timepoint of induction of (A) RosC wild-type (WT, control), (B) RosC^{D166L}, (C) RosC^{D166I} and (D) RosC^{D166V}.

levels in the cytoplasm of the recombinant strains. We tested a variety of phosphometabolites (including FMN and FAD) with regard to dephosphorylation by RosC^{D166L}, however, up to now we were not able to identify the target for this RosC variant.

Other FMN dephosphorylating enzymes are present in S. davaonensis

FMN hydrolases (EC 3.1.3.102) or acid phosphatases (EC 3.1.3.2) are enzymes, which have been studied in only very few organisms. *S.*

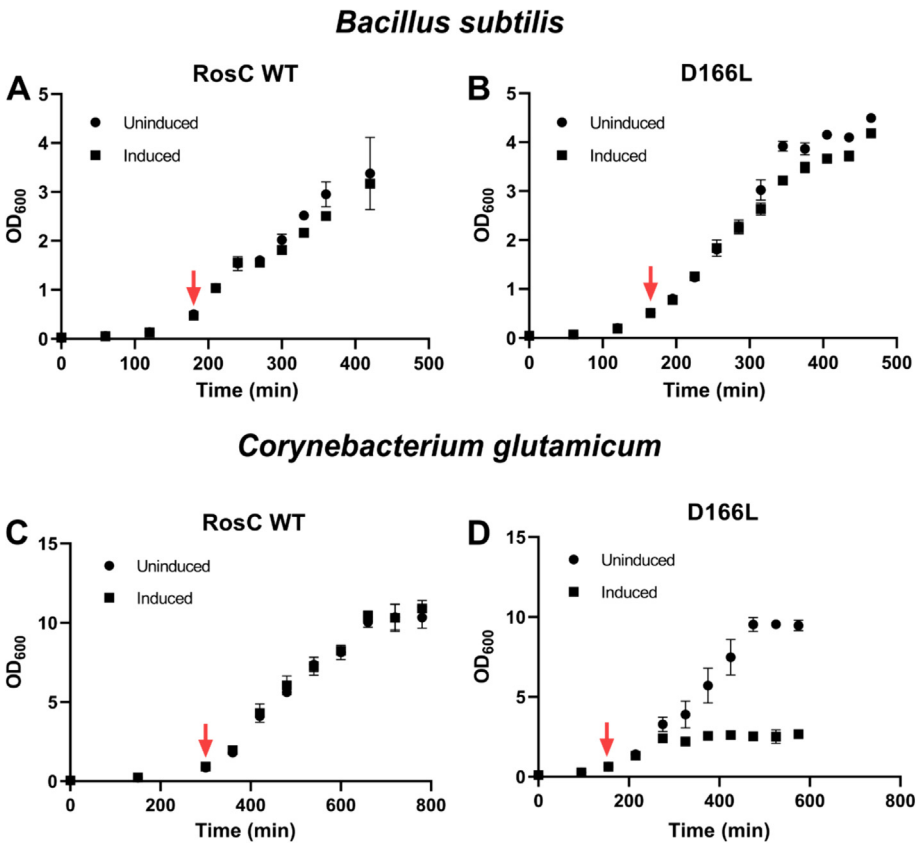

Figure 7. Overproduction of RosC^{D166L} negatively affects growth of *Corynebacterium glutamicum* but not of *Bacillus subtilis*. Growth of recombinant *B. subtilis* (A and B) and *C. glutamicum* (C and D) strains that enable overexpression of the *rosC* wild-type gene and variants was monitored. The red arrow shows the timepoint of induction. Reduced growth upon overproduction of RosC^{D166L} was only observed in *C. glutamicum* but not in *B. subtilis*. The successful overproduction of RosC^{D166L} in *B. subtilis* was validated by SDS-PAGE (Figure S12). It appears that the target metabolite for the phosphatase RosC^{D166L} is present in *E. coli* and *C. glutamicum* but not in *B. subtilis*.

davaonensis RosC formally also is an FMN hydrolase, and, although FMN is not the preferred substrate, it is one of the very few well characterized enzymes which dephosphorylate FMN. *E. coli* YigB and YbjI, belonging to the haloacid dehalogenase superfamily of enzymes,[14] preferentially dephosphorylate an intermediate of riboflavin biosynthesis, 5-amino-6-ribitylamino-2,4 (1*H*,3*H*)-pyrimidinedione 5′-phosphate (ARPP) but, interestingly, also FMN.[14] Two putative enzymes encoded by the genes BN159_4587 and BN159_0855 were identified in the genome of *S. davaonensis* by a BLASTp search using the primary structure of *E. coli* YbjI. Alphafold models[15] of BN159_4587 and BN159_0855 confirm their membership to the haloacid dehalogenase superfamily but do not show any structural similarity to RosC (Figure S14). The *S. davaonensis* genes BN159_4587 and BN159_0855 were nevertheless overexpressed in *E. coli* and the corresponding gene products were tested in cell-free extracts using FMN (Figure S15), AFP (Figure S16) and ARPP (Figure S17) as substrates. FMN appeared to be the best substrate although the other compounds were dephosphorylated as well. Notably, RosC does not dephosphorylate ARPP (Figure S17). BN159_4587 and BN159_0855 are expressed in the exponential as well as in the stationary phase[16] but the physiological roles of their gene products at present remain unclear.

Discussion

One major challenge with regard to evolving the AFP phosphatase RosC was the discrimination between the roseoflavin pathway specific intermediate AFP and the structurally similar flavin cofactor FMN as phosphorylation of riboflavin by RibCF at the expense of ATP and subsequent dephosphorylation of FMN by RosC would generate a “futile cycle” and waste cellular energy in roseoflavin producers (Figure 1). Indeed, the preferred substrate of RosC is AFP (k_{cat} = 31.3 min^{-1}; K_M = 34.5 μM; k_{cat}/K_M = 0.91 min^{-1} μM^{-1}) although FMN is also dephosphorylated albeit with a strikingly lower efficiency (k_{cat} = 7.1 min^{-1}; K_M = 309 μM; k_{cat}/

K_M = 0.023 min^{-1} μM^{-1}).[8] Still, we hypothesized that the latter activity might successfully compete with flavoproteins for FMN and also may negatively affect synthesis of FMN and FAD by the bifunctional flavokinase/FAD synthetase RibCF in *S. davaonensis*.[4] *E. coli* contains 40 different flavoproteins and the functionality of this "flavoproteome" depends on the availability of the cofactors FMN and FAD.[17,13] Flavoproteins bind flavins as cofactors with dissociation constants in the micromolar range.[18,19] In *E. coli* cytoplasmic FMN and FAD levels were determined to be 54 μM and 170 μM,[20] respectively, and thus are sufficiently high to ensure that the flavoproteome is fully loaded with FMN/FAD. It is reasonable to assume that growth of *E. coli* is negatively affected when cytoplasmic FMN and FAD levels fall below these values and we think that this is also true for the roseoflavin producing *Streptomyces* species. Limited dephosphorylation of FMN by RosC wild-type (K_M = 309 μM) and by e.g. the RosC variant $RosC^{D166E}$ (K_M = 24.5 μM) (see Table 1) apparently does not negatively affect cofactor availability in *E. coli* since growth is not reduced upon induction of these recombinant FMN phosphatases. However, reduced growth was observed when overproducing the variant $RosC^{D166L}$ in *E. coli*. The same was found in *C. glutamicum* (Figure 6) but not in *B. subtilis* (Figure 7). Analysis of the apparently toxic RosC variants $RosC^{D166L}$, $RosC^{D166I}$ and $RosC^{D166V}$ revealed that the toxicity for *E. coli* is not due to a more efficient dephosphorylation of FMN (see Table 1) but rather is likely due to dephosphorylation (?) of a yet unknown phosphometabolite. An untargeted metabolomics experiment is underway to identify this elusive phosphometabolite.

Structural and mutagenesis studies were performed to understand how RosC was "tamed" to sufficiently minimize FMN dephosphorylation. Binding of the flavin substrate AFP by RosC fundamentally differs from flavoenzymes which use flavins as cofactors. The active site of RosC which encapsulates the phosphate of AFP is present in the protein center and is highly conserved among histidine phosphatase family members (Figure S3), while the isoalloxazine part of the flavin is fixed in the periphery of the protein by three specific sections and a specialized N-terminal helical extension representing a novel flavin binding mode (Figure 2A). An in-depth comparison of the overall structure of RosC to structures of phosphatases from the same class is shown in Table S2. An overlay of RosC and its closest relative is shown in Figure S18. AFP specificity of RosC may be supported by an induced-fit process involving a pronounced rigidification event of the supplementary segments (compare Figure 2B and D). D166 plays a key role in the delicate distinction between isoelectronic AFP and FMN. D166 preferentially binds the C8 amino group of AFP (Figures 3 and 5B) and does not favorably interact with the non-polar C8 methyl of FMN. We expected that it would be straightforward to engineer an FMN dephosphorylating "killer enzyme" by replacing D166 by an amino acid with a more hydrophobic side chain. However, this did not succeed, as D166 is crucial for both substrate binding and turnover and consequently most of the $RosC^{D166}$ mutants were inactive. One step towards generating an enzyme which more favorably binds FMN was $RosC^{R33A}$, in which the distance between D166 and the amino group at C8 of AF was increased due to reorientation of the carboxylate into the free space created by the eliminated bulky R33 side chain (Figure S5). An FMN dephosphorylating enzyme, however, was also not generated as in the wild-type enzyme R33 is important for positioning the terminal phosphate of FMN and the absence of R33 fully deactivates the enzyme (Figure 4A and Table 1). A big surprise was that the $RosC^{D166E}$ variant dephosphorylated AFP significantly faster than the wild-type and that apparent binding of AFP was better (Table 2). Even more surprising was the finding that the rate of FMN turnover by $RosC^{D166E}$ was higher than in the wild-type and that the K_M was also lower for this substrate (Table 2). We speculate that the longer side chain of E166 in $RosC^{D166E}$ causes a similar rotation as found for D166 in the variant $RosC^{R33A}$ (Figure 5), which, in case FMN is the substrate, would position the methylene group of E166 of $RosC^{D166E}$ towards the C8 methyl of FMN and its carboxylate towards the ribityl hydroxyl groups of FMN. The thereby increased binding strength and FMN dephosphorylation capability is unfavorable for cellular flavin metabolism which rationalizes the strict conservation of D166 despite the lower AFP dephosphorylation rate of the wild-type compared to the variant $RosC^{E166}$. Although this is not favorable for roseoflavin biosynthesis, it provides limited protection of roseoflavin producing organisms from FMN dephosphorylation.

Experimental Procedures

Chemicals

Roseoflavin was purchased from Chemos (Regenstauf, Germany) and riboflavin was purchased from AppliChem GmbH (Darmstadt, Germany). AF was a gift from Peter Macheroux (Technical University of Graz, Austria). AFP was enzymatically synthesized as described.[2]

Bioinformatic tools

The structural alignment tools I-TASSER[21] and DALI[22] were used for mining sequences sharing structural similarity to RosC. These sequences were

used to create a sequence alignment using ClustalW.[23]

Bacterial strains and growth conditions

E. coli and *B. subtilis* cells were aerobically grown in LB at 37 °C. *C. glutamicum* was aerobically grown in brain heart infusion supplement (BHIS) medium or the minimal medium CGXII supplemented with 4% (w/v) glucose.[24]

Construction of expression plasmids

Construction of expression plasmids which were used to generate recombinant RosC overproducing *E. coli* (*Escherichia coli* BL21(DE3) pLysS), *B. subtilis* (wild-type Marburg 168; DSM 23778) and *C. glutamicum* (wild-type, ATCC 13032) strains is described in the supplement. For overexpression of the putative FMN phosphatase genes BN159_4587 and BN158_0855 *E. coli* Rosetta (DE3) was used. Site directed mutagenesis of expression plasmids to generate RosC variants overproduced in *E. coli* was carried out using the QuikChange Lightning Site-Directed Mutagenesis Kit (Agilent Technologies, Waldbronn, Germany) according to the instructions of the manufacturer. The supplement lists oligonucleotides which were employed for cloning and site-directed mutagenesis.

Purification of Strep-tagged RosC wild-type and RosC variants by affinity chromatography

Chromatographic steps were performed using the ÄKTA purifier™ system (GE Healthcare). Frozen cell pellets of *E. coli* BL21(DE3)pLysS strains overproducing N-terminally strep tagged RosC and variants thereof were resuspended in 30 ml washing buffer (100 mM Tris HCl, 150 mM NaCl, 1 mM EDTA; pH 8.0), containing a cOmplete™, EDTA-free, protease inhibitor cocktail tablet (Merck KGaA, Darmstadt, Germany). Cell free extracts were prepared using a French press (three cycles) with a pressure of 2,000 bar at 10 °C. Cell debris and unbroken cells were removed by two centrifugation steps (8,000*g*, 4 °C, 10 min followed by 108,000*g*, 4 °C, 30 min). Cell lysates were applied to a 5 ml Strep-Tactin® Superflow® high-capacity cartridge column (IBA Lifesciences, Göttingen, Germany) equilibrated with washing buffer at a flow rate of 0.5 ml per min. As soon as the UV signal returned to its baseline, elution of Strep-tagged protein was accomplished by applying a gradient of 1.67% per min (100% buffer E in 30 min) elution buffer (100 mM Tris HCl, 150 mM NaCl, 1 mM EDTA, 10 mM desthiobiotin; pH 8.0). Eluted fractions were concentrated using Vivaspin 6 centrifugal concentrators with a molecular weight cut-off of 10 KDa (Sartorius, Göttingen, Germany) at 6,000*g* and 4 °C. Eluted fractions were concentrated as described above and loaded onto a Superdex® 200 Increase 10/300 GL column (GE Healthcare) equilibrated with running buffer (10 mM Tris HCl, 150 mM NaCl; pH 7.6) at a flow rate of 0.5 ml per min. Fractions were collected, glycerol was added to a final concentration of 20% (v/v) and enzymes were stored at −20 °C. $RosC^{StrepN}$ was fully active for at least six months under these conditions. For purification of MBP-fusions from *E. coli* preparation of cell lysates and clarification steps were the same as described above. Pellets of NEBExpress® cells (New England Biolabs GmbH, Frankfurt, Germany) overproducing N-terminally MBP-fused RosC wild-type (RosC-MBP) and $RosC^{\Delta 22}$-MBP were resuspended in column buffer (20 mM Tris-HCl, 200 mM NaCl; pH 7.4) containing cOmplete™. Gravity flow columns (2 ml) containing amylose resin (New England Biolabs GmbH, Frankfurt, Germany) were loaded with 10 ml clarified cell free extracts and washed with 5 column volumes of column buffer (20 mM Tris–HCl, 200 mM NaCl; pH 7.4). Elution of MBP-fused proteins was carried out by adding elution buffer (20 mM Tris–HCl, 200 mM NaCl, 10 mM maltose; pH 7.4) in three steps. At least three fractions (1 ml each) were collected and checked with regard to their apparent homogeneity using SDS-PAGE (see below).

Enzyme assays and HPLC analysis of flavins

AFP and FMN phosphatase activity of purified RosC and variants thereof was determined in 100 mM 1,3-bis[tris(hydroxymethyl)methylamino]propane (BTP) containing 200 μM $CaCl_2$ and 5–400 μM AFP (pH 7.6). Mixtures were equilibrated at 37 °C for 5 min and reactions were started by adding 0.6–2.4 μM purified RosC. After appropriate time intervals, aliquots were removed and treated with 5% (w/v) TCA and placed on ice to stop the reaction. Samples were analyzed by high-performance liquid chromatography as described.[8] AFP and AF were detected photometrically at λ = 480 nm, FMN and riboflavin at λ = 445 nm and RoFMN and RoF at λ = 503 nm. Flavin standard stock solutions were used as references. Kinetic constants K_M and k_{cat}/V_{max} were determined by fitting the data to the Michaelis-Menten equation using nonlinear regression employing OriginPro (Version 9). ARPP was synthesized using RibD and RibG from *E. coli* and GTP as the initial substrate. Proteins encoded by genes *rosC* (BN159_4587 and BN158_0855)[25] were tested for ARPP phosphatase and FMN phosphatase activities. The ARPP phosphatase reaction was carried out in a volume of 500 μl containing 100 mM BTP containing 20 mM DTT and 8 mM $MgCl_2$ (pH 7.5). Cell free extracts of *E. coli* overproducing the putative phosphatases (0.2 mg/ml total protein) were used for the assay. The reaction mixture was incubated at 37 °C for 1 h after addition of 0.2 mg/ml of total protein. The dephosphorylated

products, ARP or riboflavin, were detected by HPLC-FLD (excitation at 410 nm, emission at 485 nm) after derivatization with diacetyl. Cell-free extracts of *E. coli* BL21 pLySs overproducing *E. coli* YbjI were used as a positive control. The FMN phosphatase assay was carried out in a volume of 500 µl containing 100 mM BTP, 200 µM $MgCl_2$ and 100 µM FMN (pH 7.5).

Crystallization of purified RosC of S. davaonensis

For crystallization purified RosC was stored in 10 mM TRIS/HCl pH 7.5 and 150 mM NaCl at a concentration of 15 mg/ml. Sitting drop experiments were performed with the Rigaku CrystalMation robot system and commercial screens of JBS HT I, II, pentaerythritol, PACT++ (Jena Bioscience), PGA (Molecular Dimension) and JCSG Core Suite I-IV (Qiagen). Crystallization experiments were performed with the flavin-free wild-type RosC, RosC incubated with 0.5 mM AF and with 0.5 mM AF and 5 mM phosphate as well as $RosC^{R33A}$ supplemented with 0.5–1.0 mM riboflavin. The corresponding crystallization conditions and cryoprotectant solutions are listed in Table S1. Data of the obtained crystals were collected at the PXII beamline at the Swiss-Light-Source, Switzerland and processed with XDS and XSCALE[26] (Table S1). The structure of RosC was determined by the molecular replacement method using PHASER[27] with a combined model of Robetta[28] and phosphoserine phosphatase (4IJ5)[29] as initial coordinates. The correction of the models and the incorporation of ligands and solvent were performed with COOT[30]. For refinement, PHENIX[31] was applied. Original cif parameter files for the substrates AF and riboflavin was produced by PHENIX-eIBOW and slightly modified according to the electron density. The structure was analyzed by COOT and MOLPROBITY.[32] Figures 2–5 were produced with Chimera.[33]

Funding and additional information

This work was funded by the German Research Foundation (DFG grant MA2510/9-3) and by the Albert und Anneliese Konanz-Stiftung of Hochschule Mannheim.

CRediT authorship contribution statement

Tanya Joshi: Investigation. **Ulrike Demmer:** Investigation. **Carmen Schneider:** Investigation. **Theresa Glaser:** Investigation. **Eberhard Warkentin:** Formal analysis. **Ulrich Ermler:** Writing – review & editing, Writing – original draft, Methodology, Formal analysis. **Matthias Mack:** Writing – review & editing, Writing – original draft, Supervision, Resources, Project administration, Methodology, Investigation, Funding acquisition, Formal analysis, Conceptualization.

DECLARATION OF COMPETING INTEREST

The authors declare that they have no known competing financial interests or personal relationships that could have appeared to influence the work reported in this paper.

Acknowledgements

We thank Hartmut Michel for continuous support, Barbara Rathmann for keeping in operation the crystallization robot and the staff of the SLS (Villigen) for help in data collection.

Appendix A. Supplementary material

Supplementary material to this article can be found online at https://doi.org/10.1016/j.jmb.2024.168734.

Received 10 June 2024;
Accepted 29 July 2024;
Available online 2 August 2024

Keywords:
Streptomyces davaonensis;
roseoflavin;
riboflavin;
antibiotics;
phosphatases

References

1. Pedrolli, D.B., Jankowitsch, F., Schwarz, J., Langer, S., Nakanishi, S., Frei, E., Mack, M., (2013). Riboflavin analogs as antiinfectives: Occurrence, mode of action, metabolism and resistance. *Curr. Pharm. Des.* **19**, 2552–2560.
2. Pedrolli, D.B., Jankowitsch, F., Schwarz, J., Langer, S., Nakanishi, S., Mack, M., (2014). Natural riboflavin analogs. *Methods Mol. Biol.*. https://doi.org/10.1007/978-1-4939-0452-5_3.
3. Liunardo, J.J., Messerli, S., Gregotsch, A.-K., Lang, S., Schlosser, K., Rückert-Reed, C., et al., (2024). Isolation, characterisation and description of the roseoflavin producer *Streptomyces berlinensis* sp. nov. *Environ. Microbiol. Rep.*. https://doi.org/10.1111/1758-2229.13266.
4. Grill, S., Busenbender, S., Pfeiffer, M., Köhler, U., Mack, M., (2008). The bifunctional flavokinase/flavin adenine dinucleotide synthetase from Streptomyces davawensis produces inactive flavin cofactors and is not involved in resistance to the antibiotic roseoflavin. *J. Bacteriol.* **190**, 1546–1553.

5. Schwarz, J., Konjik, V., Jankowitsch, F., Sandhoff, R., Mack, M., (2016). Identification of the key enzyme of roseoflavin biosynthesis. *Angew. Chem. Int. Ed.* **55**, 6103–6106.
6. Jhulki, I., Chanani, P.K., Abdelwahed, S.H., Begley, T.P., (2016). A remarkable oxidative cascade that replaces the riboflavin C8 methyl with an amino group during roseoflavin biosynthesis. *J. Am. Chem. Soc.* **138**, 8324–8327.
7. Konjik, V., Brunle, S., Demmer, U., Vanselow, A., Sandhoff, R., Ermler, U., Mack, M., (2017). The crystal structure of RosB: insights into the reaction mechanism of the first member of a family of flavodoxin-like enzymes. *Angew. Chem. Int. Ed. Engl.* **56**, 1146–1151.
8. Schneider, C., Konjik, V., Kißling, L., Mack, M., (2020). The novel phosphatase RosC catalyzes the last unknown step of roseoflavin biosynthesis in *Streptomyces davaonensis*. *Mol. Microbiol.* **114**, 609–625.
9. Jankowitsch, F., Kuhm, C., Kellner, R., Kalinowski, J., Pelzer, S., Macheroux, P., Mack, M., (2011). A novel N, N-8-amino-8-demethyl-D-riboflavin dimethyltransferase (RosA) catalyzing the two terminal steps of roseoflavin biosynthesis in *Streptomyces davawensis*. *J. Biol. Chem.* **286**, 38275–38285.
10. Rigden, D.J., (2008). The histidine phosphatase superfamily: Structure and function. *Biochem. J.* **409**, 333–348.
11. Tyagi, A., Zirak, P., Penzkofer, A., Mathes, T., Hegemann, P., Mack, M., Ghisla, S., (2009). Absorption and emission spectroscopic characterisation of 8-amino-riboflavin. *Chem. Phys.*. https://doi.org/10.1016/j.chemphys.2009.08.005.
12. Langer, S., Nakanishi, S., Mathes, T., Knaus, T., Binter, A., Macheroux, P., et al., (2013). The flavoenzyme azobenzene reductase AzoR from *Escherichia coli* binds roseoflavin mononucleotide (RoFMN) with high affinity and is less active in its RoFMN form. *Biochemistry*. https://doi.org/10.1021/bi400348d.
13. Langer, S., Hashimoto, M., Hobl, B., Mathes, T., Mack, M., (2013). Flavoproteins are potential targets for the antibiotic roseoflavin in *Escherichia coli*. *J. Bacteriol.* **195**, 4037–4045.
14. Haase, I., Sarge, S., Illarionov, B., Laudert, D., Hohmann, H.-P., Bacher, A., Fischer, M., (2013). Enzymes from the haloacid dehalogenase (HAD) superfamily catalyse the elusive dephosphorylation step of riboflavin biosynthesis. *Chembiochem (chembiochem: Eur. J. Chem. Biol.)* **14**, 2272–2275.
15. Jumper, J., Evans, R., Pritzel, A., Green, T., Figurnov, M., Ronneberger, O., et al., (2021). Highly accurate protein structure prediction with AlphaFold. *Nature*. https://doi.org/10.1038/s41586-021-03819-2.
16. Kißling, L., Schneider, C., Seibel, K., Dorjjugder, N., Busche, T., Kalinowski, J., Mack, M., (2020). The roseoflavin producer *Streptomyces davaonensis* has a high catalytic capacity and specific genetic adaptations with regard to the biosynthesis of riboflavin. *Environ. Microbiol.*. https://doi.org/10.1111/1462-2920.15066.
17. Macheroux, P., Kappes, B., Ealick, S.E., (2011). Flavogenomics–a genomic and structural view of flavin-dependent proteins. *FEBS J.*. https://doi.org/10.1111/j.1742-4658.2011.08202.x.
18. Joosten, V., van Berkel, W.J.H., (2007). Flavoenzymes. *Curr. Opin. Chem. Biol.*. https://doi.org/10.1016/j.cbpa.2007.01.010.
19. Hefti, M.H., Vervoort, J., van Berkel, W.J.H., (2003). Deflavination and reconstitution of flavoproteins. *Eur. J. Biochem.*. https://doi.org/10.1046/j.1432-1033.2003.03802.x.
20. Bennett, B.D., Kimball, E.H., Gao, M., Osterhout, R., van Dien, S.J., Rabinowitz, J.D., (2009). Absolute metabolite concentrations and implied enzyme active site occupancy in *Escherichia coli*. *Nature Chem. Biol.*. https://doi.org/10.1038/nchembio.186.
21. Roy, A., Kucukural, A., Zhang, Y., (2010). I-TASSER: a unified platform for automated protein structure and function prediction. *Nature Protoc.*. https://doi.org/10.1038/nprot.2010.5.
22. Holm, L., (2020). Using Dali for protein structure comparison. *Methods Mol. Biol. (Clifton, N.J.)*. https://doi.org/10.1007/978-1-0716-0270-6_3.
23. Thompson, J.D., Higgins, D.G., Gibson, T.J., (1994). CLUSTAL W: improving the sensitivity of progressive multiple sequence alignment through sequence weighting, position-specific gap penalties and weight matrix choice. *Nucleic Acids Res.*. https://doi.org/10.1093/nar/22.22.4673.
24. Mora-Lugo, R., Stegmüller, J., Mack, M., (2019). Metabolic engineering of roseoflavin-overproducing microorganisms. *Microb. Cell Fact.* **18**, 146.
25. Jankowitsch, F., Schwarz, J., Rückert, C., Gust, B., Szczepanowski, R., Blom, J., et al., (2012). Genome sequence of the bacterium *Streptomyces davawensis* JCM 4913 and heterologous production of the unique antibiotic roseoflavin. *J. Bacteriol.* **194**, 6818–6827.
26. Kabsch, W., (2010). Integration, scaling, space-group assignment and post-refinement. *Acta Crystallogr. D Biol. Crystallogr.*. https://doi.org/10.1107/S0907444909047374.
27. McCoy, A.J., Grosse-Kunstleve, R.W., Adams, P.D., Winn, M.D., Storoni, L.C., Read, R.J., (2007). Phaser crystallographic software. *J. Appl. Cryst.*. https://doi.org/10.1107/S0021889807021206.
28. Kim, D.E., Chivian, D., Baker, D., (2004). Protein structure prediction and analysis using the Robetta server. *Nucleic Acids Res.*. https://doi.org/10.1093/nar/gkh468.
29. Chiba, Y., Horita, S., Ohtsuka, J., Arai, H., Nagata, K., Igarashi, Y., Tanokura, M., Ishii, M., (2013). Structural units important for activity of a novel-type phosphoserine phosphatase from Hydrogenobacter thermophilus TK-6 revealed by crystal structure analysis. *J. Biol. Chem.*. https://doi.org/10.1074/jbc.M112.449561.
30. Emsley, P., Lohkamp, B., Scott, W.G., Cowtan, K., (2010). Features and development of Coot. *Acta Crystallogr. D Biol. Crystallogr.*. https://doi.org/10.1107/S0907444910007493.
31. Afonine, P.V., Grosse-Kunstleve, R.W., Echols, N., Headd, J.J., Moriarty, N.W., Mustyakimov, M., et al., (2012). Towards automated crystallographic structure refinement with phenix.refine. *Acta crystallogr. Sect. D, Biol. Crystallogr.*. https://doi.org/10.1107/S0907444912001308.
32. Davis, I.W., Leaver-Fay, A., Chen, V.B., Block, J.N., Kapral, G.J., Wang, X., et al., (2007). MolProbity: all-atom contacts and structure validation for proteins and nucleic acids. *Nucleic Acids Res.*. https://doi.org/10.1093/nar/gkm216.

33. Pettersen, E.F., Goddard, T.D., Huang, C.C., Couch, G.S., Greenblatt, D.M., Meng, E.C., Ferrin, T.E., (2004). UCSF Chimera–a visualization system for exploratory research and analysis. *J. Comput. Chem.*. https://doi.org/10.1002/jcc.20084.

34. Schneider, C., (2020). Die Phosphatase RosC katalysiert den letzten unbekannten Schritt der Roseoflavin-Biosynthese in *Streptomyces davaonensis*. KIT Karlsruhe.